

# *Analysis of the vibration impact of railway tunnel blasting excavation on existing highway tunnels*

Liao Leiyi<sup>1</sup>, Hu Qinglong<sup>2</sup>, Liu Yongjian<sup>3</sup>, Shan Yepeng<sup>3</sup>, Cai Guoqing<sup>3</sup>

<sup>1</sup>Deputy General Manager and Chief Engineer, Guangxi Liuwu Railway Co., Ltd., Nanning, 530012, China

<sup>2</sup>China Railway Engineering Design and Consulting Group Co., Ltd., Beijing, 100055, China

<sup>3</sup>School of Civil Engineering, Beijing Jiaotong University, Beijing, 100044, China

**Keywords:** Tunnel construction; Undercrossing adjacent tunnels; Midas GTX; drilling and blasting method

**Abstract:** Prior to tunnelling by drilling and blasting, a proper assessment of the impact of blasting and excavation vibrations on the adjacent existing buildings (structures) is the basis for ensuring the safe operation and maintenance of the adjacent existing buildings (structures). Based on the Zijing yaoshan Railway Tunnel under the existing Guibin highway tunnel, the Midas GTX software was used to perform non-linear time history analysis, taking into account the damping effect of the blast wave, to study the impact of tunnel blasts on existing structures. The simulation results show that the maximum vibration velocity occurs at the left wall position of the tunnel, with a size of 0.71cm/s, which meets the requirement of particle vibration velocity less than 10cm/s in the specification; Due to the plane intersection angle between the Guibin highway tunnel and the Zijing yaoshan tunnel excavated by blasting, the entire Guibin highway tunnel leans to the right, causing the left side of the Guibin highway tunnel to be affected by the blasting shock wave earlier than the right side. The vibration velocity distribution shows that the vibration velocity at the measurement point on the left side of the tunnel section is significantly higher than that on the right side; Analyzing the development curve of blasting vibration speed, the development curve can be divided into three stages, namely the rising stage, the falling stage, and the stable attenuation stage, and analyzing the characteristics of each stage.

## 1. Introduction

When the drilling and blasting method is applied to tunnel excavation, the impact of disturbance on the tunnel surrounding rock or nearby buildings can not be ignored. In order to eliminate potential safety hazards, blasting excavation needs to strictly control the maximum dosage and other relevant blasting parameters, monitoring and preventing the tunnel nearby structures. Therefore, the study of the impact of tunnel blasting and excavation on nearby existing buildings is the key to ensure the safety of existing buildings

A number of studies on vibration analysis of near structures through drilling-and-blasting method were carried out. Based on the blasting dynamic analysis and weighted double-shear strength criterion, Liu et al <sup>[1]</sup> studied the impact of ultra-close blasting on existing tunnels, and proposed the nearby

blasting safety assessment and blasting scheme preference method. Huang et al [2] used ABAQUS to establish the Zhuji tunnel model, exploring the impact of different blasting loads on the constructed small-clearance tunnels. It concluded that the blasting construction of the under-construction tunnels had the greatest impact on the vaults of existing tunnels. Wu et al [3] established a tunnel blasting finite element model, which studied the dynamic response of shallow buried tunnel lining structure, and simulated the dynamic response of the tunnel lining structure with soft body analysis. Yang et al [4] used ABAQUS finite element software to simulate the stress distribution around the borehole, and analysed the sensitivity of different depths, different sizes of the boring face, and different lithologies on the distribution of horizontal stresses. Xu et al [5] coupled the tensile and compressive weighted damage variables with the classical PLASTIC-KINEMATIC model to establish a constitutive model of rock blasting damage. The model was used for numerical simulation of tunnel slotted blasting to study the evolution of rock damage in the process of slotted blasting construction. Qing et al [6] used numerical simulation to study the vibration propagation and the Peak Plasma Velocity (PPV) distribution of the near lining in the tunnel blasting process, indicating that the vibration velocity along the direction of the tunnel direction is the largest, which plays an important role in the vibration of near tunnels. In summary, the current study lacks comparative analyses of monitoring at different locations of existing tunnels and the effect of blasting parameters on the vibration response of existing tunnels.

In this paper, based on the blasting and excavation project of Zijingyao Mountain Tunnel of Liuwu Railway, Midas GTX software is used to carry out nonlinear time-range analysis of the tunnel structure. By monitoring the vibration velocity of the existing tunnels at different distances and at different locations, the attenuation effect of the blast wave was explored, and the safety of the existing tunnels was evaluated. In addition, by analysing the decay curves of the vibration velocity with time at different locations, the relevant laws of the vibration velocity development curve are derived.

## 2. Overview of the project

Liuwu railway starting station is Jinde station, which is Liuzhou railway junction, and the terminal is Wuzhou station, the total length of the line is 237.8 km. From which, Zijingyao Mountain tunnel is located in Laibin City, the Guangxi Zhuang Autonomous Region and Guigang City. Starting and ending mileage of the tunnel: DK95+732 ~ DK104+620 with a total length of 8888 m. It is a single-cavity, two-lane tunnel. Zijing Yaoshan tunnel is passing through the Guibin Tunnel of Pingwu Expressway, with a depth of 284 m. The tunnel is covered by three layers of rocks consist of 10 m fully weathered sandstone, 40 m strongly weathered sandstone, and 234 m weakly weathered sandstone. The clear distance between Zijingyao Mountain tunnel and Guibin tunnel structure is about 65.48 m, the plane intersection angle is  $20^\circ$ , as shown in Fig. 1 and Fig. 2.

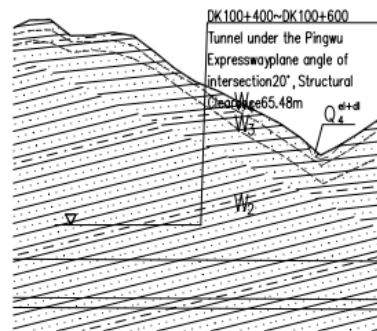
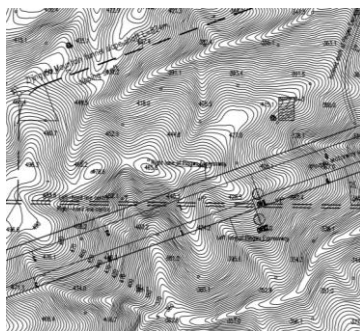


Figure 1: Schematic plane of the Guibin tunnel underneath the main tunnel of Zijingyao Mountain tunnel      Figure 2: Schematic section of the Guibin tunnel underneath the main tunnel of Zijingyao Mountain tunnel

In the underpass section of the tunnel, an in-cavity overrun long pipe shed was used for overrun pre-support reinforcement, and drilling and blasting methods (controlled blasting, weak vibration, and surface blasting) were used for excavation. Plastic detonator non-electric millisecond micro-differential sequential detonation to reduce the impact of blasting vibration on the Guibin tunnel structure. The construction process can be seen in Fig. 3 below.

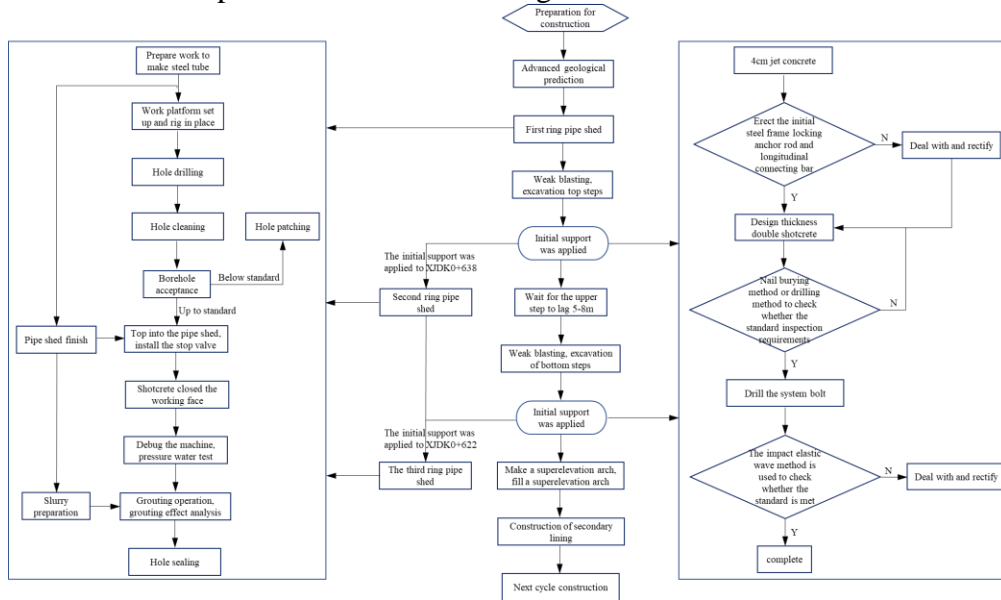


Figure 3: Flow chart of underpass construction

The section of Zijingyao Mountain tunnel adopts three-centred circle, the radius of the arch is  $r_1 = 5.31m$ , the arc range is  $120^\circ$ ; the radius of the side wall is  $r_2 = 7.66m$ , the arc range is  $46^\circ$ ; the radius of the super-elevation arch is  $r_3 = 11.85m$ , the arc range is  $37^\circ$ , the dimensions of the tunnel section are shown in Fig. 4. The cross-section of the Guibin tunnel is shown in Fig. 5, which is a two-bore road tunnel with a distance of 32 m between of the left and right holes along the centre line, the diameter of 13.68 m for a single hole.

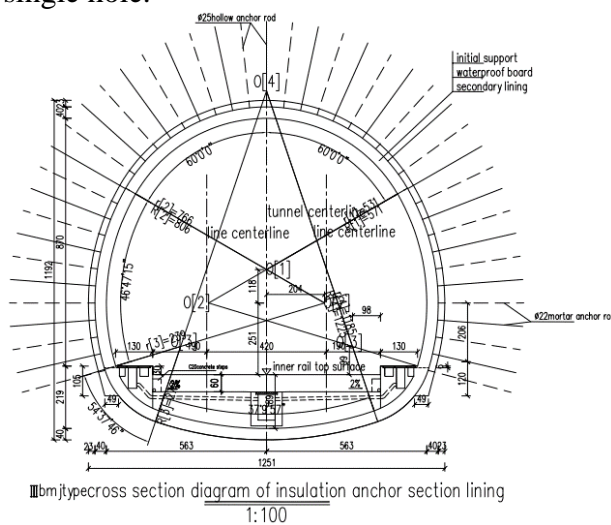


Figure 4: Tunnel cross-section

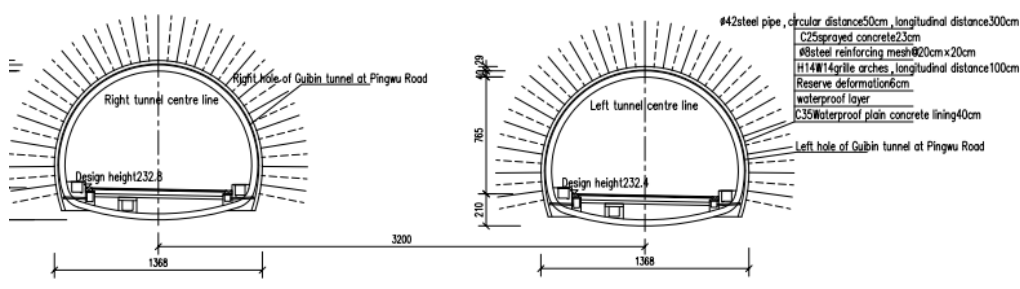


Figure 5: Cross-section of Guibin tunnel

### 3. Modelling process and parameters

Numerical simulation of tunnel blasting and excavation is carried out by Midas GTX during the whole process of tunnel excavation to study the impact of blasting and excavation of Zijingyao Mountain Tunnel on the Guibin tunnel located above it. The Mohr Coulomb constitutive model is adopted, which is an ideal elastic-plastic model that combines Hooke's law and the Cullen damage criterion. There are five parameters consists of two elastic parameters, i.e modulus of elasticity  $E$  and Poisson's ratio, and three plastic parameters, i.e effective cohesion  $c$ , effective angle of internal friction and angle of dilation. The Mohr Coulomb model adopts elasto-plasticity theory, which provides a better description of the damage behaviour of soils.

#### 3.1 Geotechnical bodies and support structures

The model adopts three-dimensional modelling method, with three-dimensional solid units for the strata and plate units for the spray mix. According to St. Venant's principle, the size of the modelled geotechnical body is generally larger than three times the diameter of the tunnel [7]. Combined with geological investigation data and construction data, the modelling material parameters of Zijingyao Mountain Tunnel can be obtained as shown in Table 1.

Table 1: Modelling parameters of Zijingyao Mountain tunnel

position	materials	calculation model	modulus of elasticity /kPa	weight capacity /(kN/m <sup>3</sup> )	Poisson's ratio	cohesive force /kPa	friction angle /(°)
rock and soil	fully weathered sandstone	Mohr Coulomb	$2.0 \times 10^7$	20	0.3	28	18
	strongly weathered sandstone		$2.4 \times 10^7$	20	0.3	80	18
	weakly weathered sandstone		$2.8 \times 10^7$	20	0.3	90	19
Pipe Shelter Reinforcement Area	weakly weathered sandstone		$4.5 \times 10^7$	20	0.3	100	24
Initial support/temporary support	C25	elastin	$2.8 \times 10^7$	25	0.20	\	\
anchor	steels	elastin	$2.1 \times 10^8$	78.5	0.28	\	\

In the proposed geotechnical model, the thickness of the soil layer and the spatial relationship between the two tunnels are shown in Fig. 6, the model length along boring direction is 200m, the width 200m, the height 350 m. The geotechnical body mesh adopts tetrahedral plus hexahedral hybrid mesh, the geotechnical body mesh limitation size is 20 m, and the mesh limitation size of the soil body in the tunnel excavation is 2 m. The spray hybrid mesh is generated by analytical extraction to ensure the coupling of each node, and there are 29509 nodes and 58123 cells in the generated model.

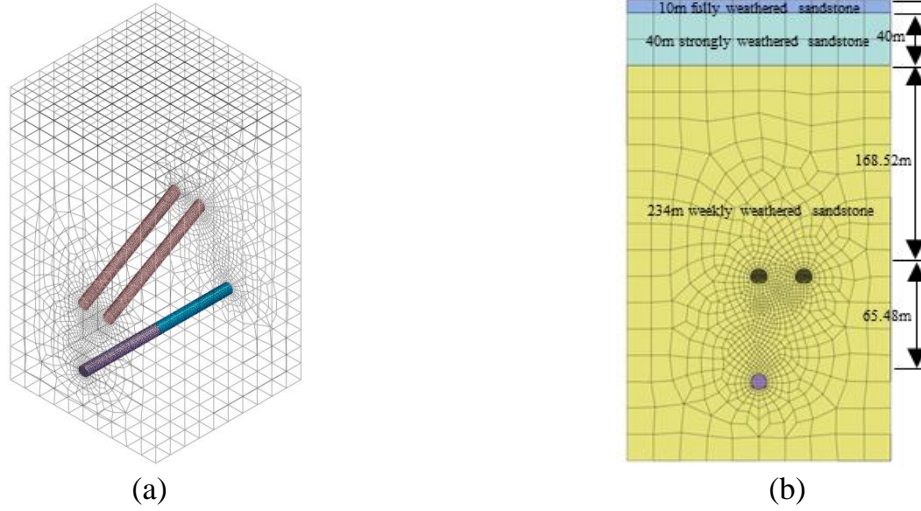


Figure 6: Model of geotechnical body under Baomao Expressway

### 3.2 Boundary conditions

Lysmer and Wass<sup>[8]</sup> suggested the use of viscoelastic boundaries. The specific method is firstly to simulate the elastic boundary by establishing the surface spring, and then to obtain the eigenperiod and eigenfrequency of the geotechnical body through eigenvalue analysis, the spring coefficients of the elastic boundary can be calculated by the foundation reaction coefficients of the road design specification<sup>[9,10]</sup>.

$$k_y = k_{y0} \cdot \left(\frac{B_y}{30}\right)^{-3/4} \quad (1)$$

$$k_{y0} = \frac{1}{30} \alpha E_0 \quad (2)$$

$$B_y = \sqrt{A_y} \quad (3)$$

where,  $A_y$  is the cross-sectional area of the geotechnical body along the vertical direction, its unit is  $cm^2$ .  $B_y$  is the equivalent length along the vertical direction with unit of  $cm$ ,  $E_0$  is the modulus of elasticity with unit of  $N/cm^2$ ,  $\alpha$  is taken to be 1.0,  $k_{y0}$  is an intermediate calculation parameter.  $k_y$  is the coefficient of foundation reaction along the vertical direction, and the coefficients of foundation reaction in the other directions are also calculated in the same way.

Based on Eqs (1) to (3) above, the reaction coefficients of the foundations are obtained. Since the thickness of the first two layers of overburden is much less than that of the third layer, it can be calculated as weakly weathered sandstone, and the results of the calculations are shown in Table 2

below.

Table 2: Calculation of Foundation Reaction Factors

Calculation steps	x	y	z
cross-sectional area $A/\text{cm}^2$	$A_x=2 \times 10^4 \times 3.5 \times 10^4=7 \times 10^8$	$A_y=2 \times 10^4 \times 3.5 \times 10^4=7 \times 10^8$	$A_z=2 \times 10^4 \times 2 \times 10^4=4 \times 10^8$
$B/\text{cm}$	$B_x=\sqrt{7 \times 10^8}=26457$	$B_y=\sqrt{7 \times 10^8}=26457$	$B_z=\sqrt{4 \times 10^8}=20000$
$k_0/\text{N}/\text{cm}^2$	$4.5 \times 10^6 / 30 = 93333$		
$k/\text{kN}/\text{m}^3$	$k_x = k_0 \cdot \left(\frac{B_x}{30}\right)^{-3/4} = 576727$	$k_y = k_0 \cdot \left(\frac{B_y}{30}\right)^{-3/4} = 576727$	$k_z = k_0 \cdot \left(\frac{B_z}{30}\right)^{-3/4} = 711383$

The viscous boundary is defined by calculating the damping ratio in each direction of the corresponding geotechnical body, which is calculated through the following equation.

Damping corresponding to P-wave

$$C_p = \rho \cdot A \sqrt{\frac{\lambda + 2G}{\rho}} = w \cdot A \sqrt{\frac{\lambda + 2G}{9.18w}} = c_p \cdot A \quad (4)$$

Damping corresponding to the S-wave

$$C_s = \rho \cdot A \sqrt{\frac{G}{\rho}} = w \cdot A \sqrt{\frac{G}{9.18w}} = c_s \cdot A \quad (5)$$

$$\lambda = \frac{\nu E}{(1 + \nu)(1 - 2\nu)} \quad (6)$$

$$G = \frac{E}{2(1 + \nu)} \quad (7)$$

Where,  $\lambda$  is the volume elasticity coefficient with unit of  $\text{kPa}$ ,  $G$  is the shear elasticity coefficient with unit of  $\text{kPa}$ ,  $E$  is the modulus of elasticity with unit of  $\text{kPa}$ ,  $\nu$  is the Poisson's ratio,  $A$  is the cross-sectional area with unit of  $\text{m}^2$ ,  $\rho$  is the density of the soil with unit of  $\text{kg}/\text{m}^3$ ,  $C_p$  is the damping corresponding to the P-wave in the soil;  $C_s$  is the damping corresponding to the S-wave in the soil;  $w$  is the gravity of the soil with unit of  $\text{kg}/\text{m}^3$ . According to Eqs. (4) to (7), the damping ratio of the soil body is  $c_p = 274562$ ,  $c_s = 146760$ .

### 3.3 Blasting loads

According to the blast load calculation formula of The International Society of Explosives Engineers (ISEE), the blast load per 1 kg is calculated as shown below.

$$P_{\text{det}} = \frac{4.18 \times 10^{-7} \times S_{\text{ge}} \times V_e^2}{1 + 0.8 S_{\text{ge}}} \quad (8)$$

$$P_B = P_{det} \times \left(\frac{d_c}{d_h}\right)^3 \quad (9)$$

$$P_D(t) = 4P_B \left( \exp\left(\frac{-Bt}{\sqrt{2}}\right) - \exp(-\sqrt{2}Bt) \right) \quad (10)$$

Where  $P_{det}$  is the blasting pressure,  $P_B$  is the pressure on the hole wall surface,  $V_e$  is the blasting velocity,  $d_c$  is the powder diameter,  $d_h$  is the diameter of the eyelet,  $S_{ge}$  is the specific gravity of the explosive;  $B=16338$  is the load constant,  $t$  is the time.

According to the relevant construction program,  $\Phi 32 \text{ mm} \times 300 \text{ mm}$  rock emulsion explosives are adopted, the density of which is  $1.05 \text{ g/cm}^3$ , detonation velocity is  $3500 \sim 5000 \text{ m/s}$ , the diameter of the borehole is taken as  $50 \text{ mm}$ . The blast load calculated based on Eqs. (8) to (10), which is determined by the charge volume, is shown in Fig. 7 below.

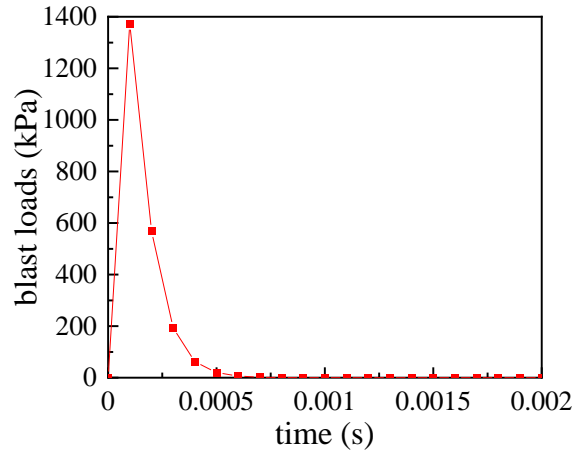


Figure 7: Generated blast loads

The layout of the boreholes in the construction program is shown in Fig. 8. In the numerical simulation, the main consideration is the impact of the blasting load on the surrounding surrounding rock, ignoring the destructive effect on the soil, so the blast load is applied to the surrounding cave wall at each blasting, as shown in Fig. 9.

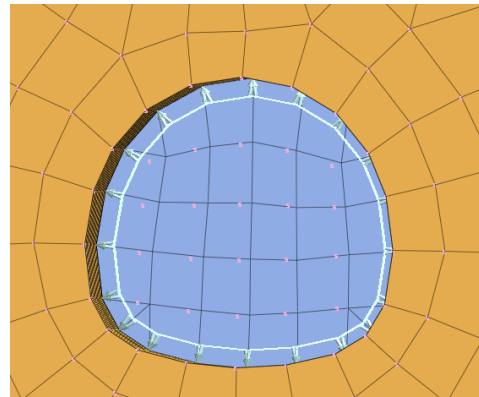
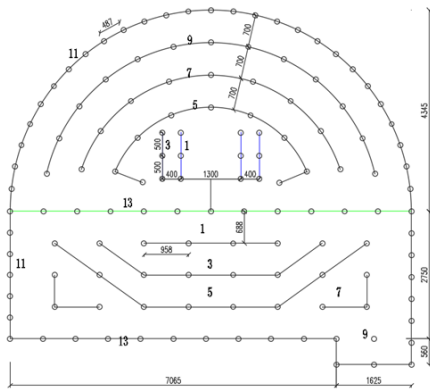


Figure 8: Zijingyao Mountain tunnel borehole layout under Guibin tunnel section      Figure 9: Location of blast load application

### 3.4 Simulated working condition setup

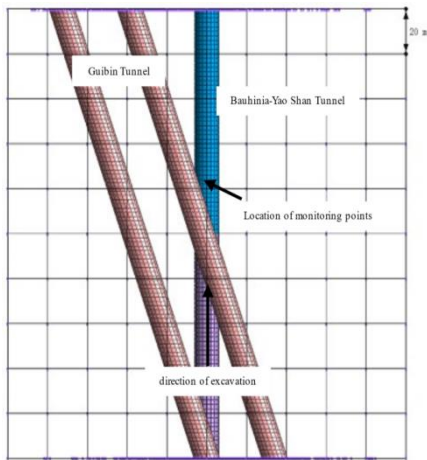


Figure 10: Layout of measurement points

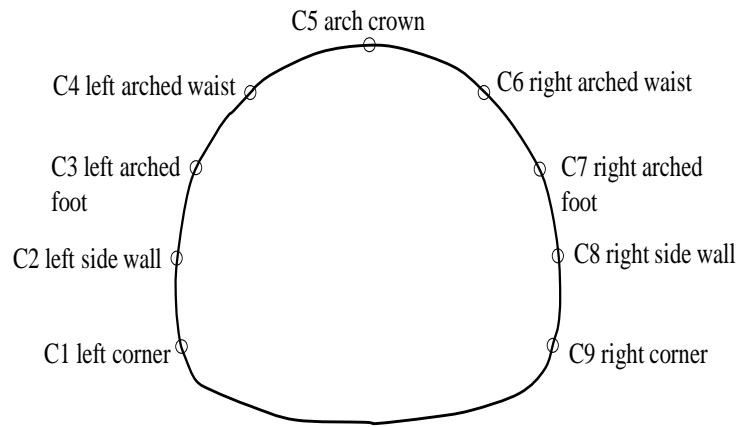


Figure 11: Layout of Monitoring Points in the Guibin tunnel

As shown in Fig. 10, which is the top view of the model, the Guibin tunnel is marked in red, and the perpendicular to the boundary plane of the geotechnical body is the Zijingyao Mountain tunnel. The numerical simulation condition is set to simulate blasting per 20 m along the excavation direction, and the blasting velocity at the intersection of the Guibin tunnel and Zijingyao Mountain is monitored. The arrangement of the vibration velocity monitoring points in the Guibin tunnel is shown in Fig. 11, and 9 tunnel section monitoring points are set up to monitor the key nodes of the tunnel section.

## 4. Dynamic response trait analysis

### 4.1 Distribution of Peak Velocity of Plasmas

Monitoring points are set up every 20 m at intervals of 80 m from the location of the explosion source. The vibration velocity of monitoring points are collected, which is shown in Fig.12.

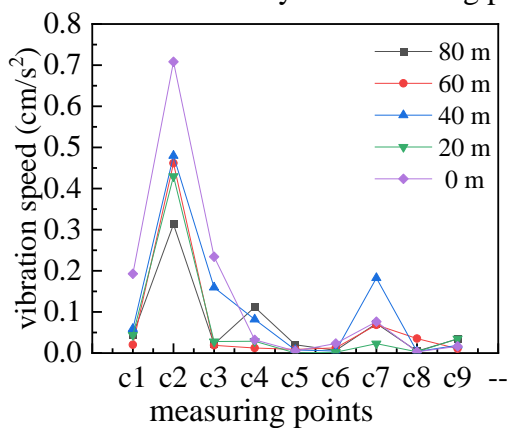


Figure 12: Vibration velocities at different blasting distances for different measurement points.

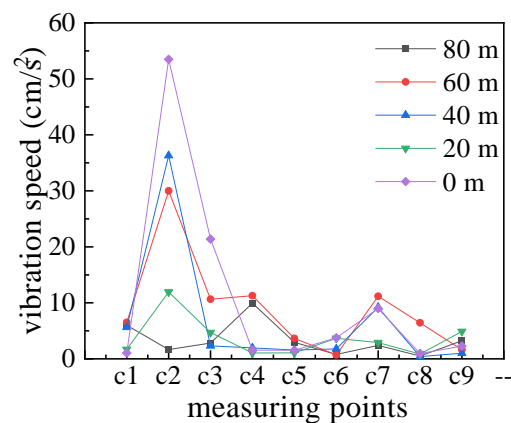


Figure 13: Vibration acceleration at different points for different blasting distances.

From Fig. 12, it can be seen that in the case of blasting excavation underneath the existing Guibin tunnel, the location of the largest vibration velocity occurs at the location of the left wall, with a size of 0.71 cm/s, which is lower than the limit value of the vibration velocity of the mass point for the traffic tunnel by 10 cm/s, based on the provisions of the "Railway Tunnel Monitoring and Measuring

Technical Specification". The vibration velocity at the right arch foot position is larger, and the vibration velocity at the arch top is the smallest. We can also find that the vibration velocity of the left measurement point is obviously larger than that of the right side. This is due to the fact that the intersection angle between the Guibin tunnel and the blasting excavation of the Zijingyao Mountain tunnel is 20 °, and the Guibin tunnel as a whole is deviated to the right side (see Fig. 10), which makes the left side of the tunnel to be affected by the blasting shock wave faster than the right side. In addition, the closer the blasting point is to the monitoring point, the higher the vibration velocity is at the measuring points with the same orientation.

#### 4.2 Distribution of vibration acceleration

The peak vibration accelerations at different measurement points with different blasting distances are shown in Fig. 13. When blasting directly above the Guibin Tunnel, the vibration acceleration of the mass on the left wall of c2 is the largest, which is about 55 cm/s<sup>2</sup>, the vibration acceleration of the mass at the Guibin tunnel decreases rapidly with the blasting of the Zijingyao Mountain tunnel moves forward, while the other masses rises slightly. It is found that the acceleration has obvious amplification effect and the corresponding vibration period is extremely short, so the tunnel safety of the c2 mass needs to be paid close attention. Acceleration can reflect the mechanical effect of seismic waves on existing buildings, however, compared with the vibration velocity of the ground mass, the dispersion of acceleration and displacement is significant, it is more reasonable to use the vibration velocity as a safety criterion.

#### 4.3 Development of the vibrational velocity of the mass with time

At different detonation distances, the vibration velocity of the monitoring point with time is studied, as shown in Fig. 14. The development curve of vibration velocity over time can be divided into three stages i.e, the rising section, the falling section and the smooth attenuation section. In the rising section, the vibration velocity of the mass increases rapidly and reaches a peak in an extremely short period of time (typically 2 to 4 ms). In the descending section, due to the very short duration of the blast load, the vibration velocity of the mass also decreases relatively quickly, generally to a vibration velocity of 0.1 cm/s within 6-10 ms. In the steady decay section, the blasting load effect is basically over, and the velocity of the mass gradually decays to 0 cm/s under the effect of soil damping, the process usually lasts for about 20 ms.

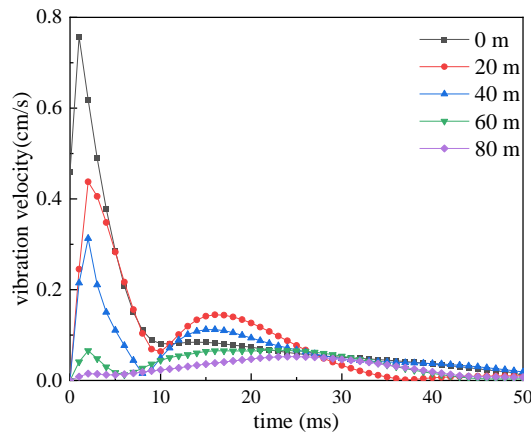


Figure 14: Decay of Burst Vibration Velocity with time

## 4.4 Blasting shock wave propagation

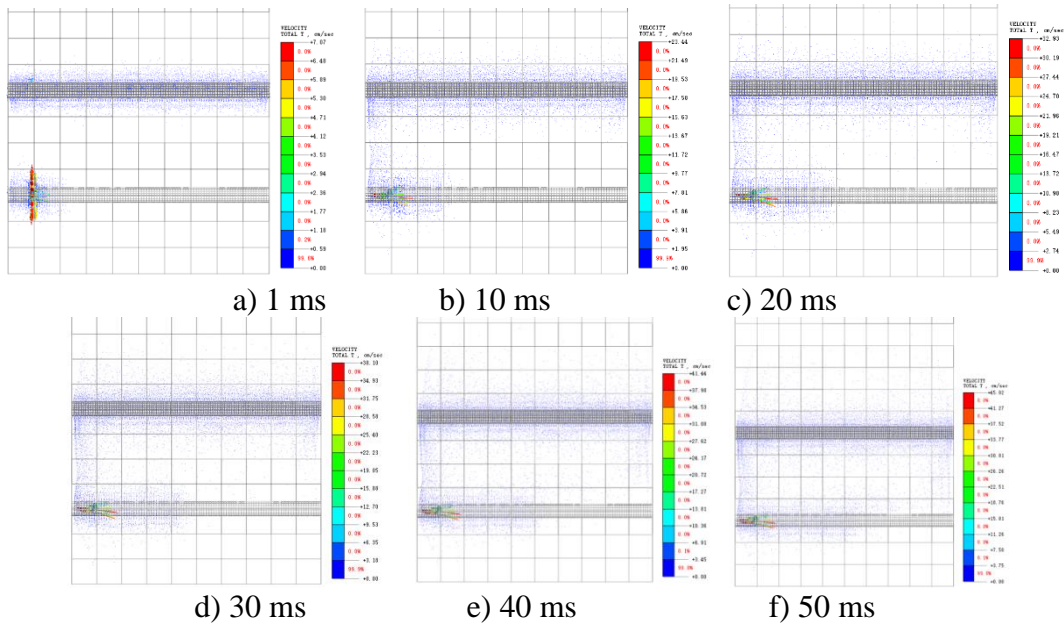


Figure 15: Vector diagram of the vibration velocity of the mass point

Fig. 15 represents the velocity vector diagram of the measuring point after 1ms, 10ms, 20ms, 30ms, 40ms and 50ms of vibration blasting, which reflects the vibration of the measuring point 80 metres away from the source of the blast. 1 ms after the occurrence of blasting, it is found that the loading surface, ie, the mass on the rock wall, has a larger vibration velocity, the direction of which along the radial direction of the rock wall outward. The existing Guibin Tunnel in the vicinity of the location of the blasting also occurred in a larger mass vibration, which in turn makes the lining of the back of the Guibin tunnel to vibrate. Explosion shock wave propagated backward with time in Zijingyao Mountain tunnel, the blue arrow after the excavation direction gradually increased until it covered the entire geotechnical body. Because of the limitation of the geotechnical body behind, the direction of vibration for the mass at the location of the blasting location also began to reverse, and the velocity of vibration began to attenuate.

## 5. Conclusion

Numerical simulation study on the blasting excavation of Zijingyao Mountain tunnel under the Guibin tunnel can be concluded as follows:

(1) The existing Guibin tunnel section sets up 9 monitoring points at different locations, the largest vibration velocity in the left wall location, which is 0.71 cm/s, meeting the specification requirements that existing tunnels of the mass vibration velocity less than 10 cm/s.

(2) Analysing the vibration velocity of the mass point, it is found that, in the same tunnel section, the vibration velocity of the left measurement point was obviously larger than that of the right side, probably due to the plane angle of intersection between the Guibin tunnel and the Zijingyao tunnel, and the overall deviation of the Guibin tunnel to the right, which made the left side of the Guibin tunnel to be affected by the blast shock wave earlier than the right side.

(3) By analysing the blast vibration velocity curve, the curve is divided into three stages, ie., the rising stage, the falling stage and the steady decay stage. The blast wave is most likely to cause damage to the existing tunnel at the rising stage and the falling stage, so it is necessary to pay attention to the state of the existing tunnel in the time of 10 ms after the blast.

## References

- [1] Liu Guohua, Wang Zhenyu. Dynamic response and blast resistance analysis of tunnels under blasting load[J]. *Journal of Zhejiang University (Engineering Edition)*, 2004, 38(2): 204-209.
- [2] Huang Haibin, Li Peng, Wang Chuang, et al. Research and analysis on the influence of small clear distance drilling and blasting method on the existing tunnel structure[J]. *Advances in Civil Engineering*, 2021, 4730936.
- [3] Wu Bo, Cui Yaozhong, Meng Guowang, et al. Research on dynamic response of shallow buried tunnel lining constructed by drilling and blasting method[J]. *Advances in Materials Science and Engineering*, 2022, 4254690.
- [4] Yang Liyun, Chen Siyu, Dong Pengxiang, et al. Orthogonal analysis and numerical simulation of rock mechanics parameters in stress field of shaft heading face[J]. *Advances in Materials Science and Engineering*, 2020, 3107364.
- [5] Xu Jiancong, Wang Zelong, Rui Guorong. Tunnel slotting-blasting numerical modeling using rock tension-compression coupling damage algorithm[J]. *Applied Sciences*, 2022, 12(13): 6714.
- [6] Qin Zixiu, Zhao Yihan, Lu Chen, et al. Propagation characteristics and control technology of blasting vibration in neighborhood tunnel[J]. *Frontiers in Earth Science*, 2023, 11, 1204450.
- [7] Ye Fei, He Chuan, Xia Yongxu. Tracking monitoring and analyzing research on road tunnel lining cracks[J]. *Journal of Civil Engineering*, 2010, 43(7): 97-104.
- [8] John L, Ginter W. Shear Waves in Plane Infinite Structures[J]. *Journal of the Engineering Mechanics Division*, 1972, 98(1).
- [9] Li Rongqing, Gong Jinxin, Yang Limin. Reliability analysis of sheet pile structure[J]. *Journal of Water Resources*, 2007(10): 1265-1271.
- [10] Xie Xiaofeng, Wu Congshi, Deng Xiaozhao, et al. Study on the impact of blasting vibration on existing tunnels in underpass tunnels [J]. *Chinese and Foreign Highway*, 2013, 33(6): 208-212.